CHEMISTRY & CHEMICAL TECHNOLOGY

Chem. Chem. Technol., 2023,
Vol. 17, No. 4, pp. 719–728

Chemistry

NEW SOLID-SOLUTIONS OF SUBSTITUTION STRONTIUM (Sr) FOR LEAD (Pb) IN APATITE STRUCTURE

***Mohammed A. B. Abdul Jabar*[1,✉]**

https://doi.org/10.23939/chcht17.04.719

Abstract. Strontium substitution for lead in $Pb_{(8-x)}Sr_xNa_2(PO_4)_6$ was analyzed using XRD, SEM, and Rietveld refinement techniques. All samples were synthesized using ceramic and semi-ceramic technologies. Pure apatite was formed in the composition from x=0.00 up to x=2.75. The results indicate that the samples' collected compositions agree with the values calculated.

Keywords: lead, apatite, ceramic, semi-ceramic, solid solution.

1. Introduction

A key aspect of compounds with apatite structures is isomorphic substitutions. The study of isomorphism is one of the fundamental aspects of apatite structures since these structures are easily substituted by other atoms, ions, or molecules.[1-4] Introducing isomorphic additives into the crystal structure can change the crystal-chemical characteristics and the properties of resulting compounds or solid solutions. Therefore, modifying compounds are widely used to develop new substances with new properties. As a result, their application area may be extended significantly.[5-9] Lead apatite structures attract the attention of scientists all over the world due to their application in various scientific and technological fields. They are mainly used as reaction catalysts, luminescent materials, luminophores, and moisture and alcohol sensors. Solid solutions of lead apatite have laser properties.[10-12]

Many studies have examined various lead apatite structures (space group P63/m). The first type of lead apatite has the formula $Pb_{10}(GO_4)_6X_2$, where G = P^{5+}, V^{5+}, As^{5+}, and X = hydroxyl group (OH^-), halogen anions (F^-, Cl^-, Br^- and I) and □ (anion vacancy). Lead-hydroxyapatite $Pb_{10}(PO_4)_6(OH)_2$) was studied by solid solution reaction and precipitation methods. In many studies, lead-hydroxyapatite solid solution system ($Pb_{10}(PO_4)_6(OH)_2$) was prepared and calcined at different temperatures: 37, 80, 100, 300, 425, 600, and 900 °C or kept at 40 °C for seven days.[13-19] By precipitating process, pyromorphite, $Pb_{10}(PO_4)_6Cl_2$, and mimetite, $Pb_{10}(AsO_4)_6Cl_2$ structures were synthesized at 298 K.[20] Lead bromoapatite, [$Pb_{10}(PO_4)_6Br_2$], has been synthesized by ceramic method (solid-state reaction) at the temperature of 900 °C for 20 hours or 750 °C for 87 hours and pressure of 1.0 GPa.[21] Lead fluorapatite, $Pb_{10}(PO_4)_6F_2$ was synthesized in a conventional muffle furnace at the temperature of 1237 °C [22] or 1000 °C for 10 hours.[23] Other structures, such as hydroxyvanadinite, $Pb_{10}(VO_4)_6(OH)_2$, were synthesized *via* the precipitation method,[24] vanadinite [$Pb_{10}(VO_4)_6Cl_2$] was synthesized at the pressure of 7.67 GPa under hydrostatic conditions,[25] and lead vanadoiodoapatite $Pb_{10}(VO_4)_6I_2$ was prepared at 800 K under thermal conditions.[26]

The second type of lead apatite with space group P63/m has the formula $Pb_8A_2(GO_4)_6$, where A = Na, K, Rb, Cs, Tl, Ag, and G = P, V, As, while X anions in their composition are absent. Silver lead apatite system $Pb_8Ag_2(PO_4)_6$ at the temperature of 215 °C and pressure of 10 MPa was obtained by hydrothermal processes.[27] Lead sodium apatite with the structures $Pb_8Na_2(PO_4)_6$, $Pb_{(8-x)}Ln_xNa_2(GO_4)_6$, $Pb_{(8-x)}Ln_xNa_2(GO_4)_6O_{(x/2)}$ and $Pb_{(8-x)}Ln_xNa_2(GO_4)_6□_{(2-x/2)}O_{(x/2)}$, (G = P^{5+}, V^{5+} and Ln = rare earth elements), were synthesized and reported in many studies. According to the solid-state method, the lead sodium apatite $Pb_8Na_2(PO_4)_6$ was synthesized at 500 °C for three days, then the temperature was increased to 1000 °C for 12 hours, and finally it was decreased to 500 °C.[28] In other works,[29-31] lead sodium apatite compounds $Pb_{(8-x)}Ln_xNa_2(PO_4)_6O_{(x/2)}$ and $Pb_{(8-x)}Ln_xNa_2(GO_4)_6□_{(2-x/2)}O_{(x/2)}$ were obtained by solid-state method with a large variety of rare earth element substitutions (La, Pr, Nd, Sm, Eu, Gd, Tb, Dy, Ho, Tm, Yb, Y) for lead (Pb). The calcined time ranged from 7 hours at 900 °C to 50–250 hours at 800 °C. Samarium substitution (Sm) for lead (Pb) in lead sodium vanadate $Pb_{(8-x)}Sm_xNa_2(VO_4)_6O_{(x/2)}$ has been investigated as well.[32] This apatite was synthesized via solid-state reaction at 600 °C for 67 hours.

Several studies have been conducted to synthesize the crystal structure of lead-strontium hydroxyapatite:

[1] College of Science, Al-Karkh University of Science, Hayfa Street, Baghdad 10001, Iraq
✉ *mohammed.a.baset1980@gmail.com*

Strontium and lead hydroxyapatite $Sr_{(10-x)}Pb_x(PO_4)_6(OH)_2$ ($0 \le x \le 10$) was precipitated and dried for 12 hours at 100 °C before being annealed for 4 hours at 600 °C.[33] Strontium-lead hydroxyapatite has the formula $Pb_xSr_{(1-x)}Ca_9(PO_4)_6(OH)_2$ ($0 \le x \le 1$). These solid solutions are obtained at 160 °C for 12 hours under hydrothermal conditions.[34] At the same time, there are no studies or data for lead-strontium sodium apatite crystal structures with the formula $Pb_{8-x}Sr_xNa_2(PO_4)_6$, which is synthesized due to the substitution of strontium for lead in Lead Sodium Apatite Structure $Pb_8Na_2(PO_4)_6$.

Therefore, this work aims to synthesize and analyze isomorphism substitutions Sr for Pb in the $Pb_{8-x}Sr_xNa_2(PO_4)_6$ composition system ($0 \le x \le 4$).

2. Experimental

2.1. Materials

Solid solution samples of system $Pb_{8-x}Sr_xNa_2(PO_4)_6$, where x = 0.00; 0.50; 1.00; 1.50; 2.00; 2.75; 3.00; 3.50 and 4.00 were prepared and synthesized by two methods: ceramic and semi ceramic methods. To obtain the isomorphism substitution of solid solutions system $Pb_{8-x}Sr_xNa_2(PO_4)_6$, we used chemically pure Lead(II) oxide (PbO), sodium carbonate (Na_2CO_3), nitric acid (HNO_3), and ammonium nitrate (NH_4NO_3). Strontium carbonate ($SrCO_3$) and ammonium phosphate ($(NH_4)_2HPO_4$) were of analytical grade, and glycerol ($C_3H_8O_3$) was Class 9. All these materials were weighed on an electronic analytical balance with an accuracy of ±0.2 mg immediately before loading. Na_2CO_3 and $SrCO_3$ were calcinated at 500 °C for 3 hours to remove adsorbed water and cooled to room temperature in a desiccator with freshly calcined silica gel.

2.2. Instrumentation

DRON-3 M diffractometer (CuKα radiation and Ni filter) with electronic control was used to analyze the synthesized samples in the X-ray phase. To determine the phase composition of the samples obtained the diffraction patterns were taken at a counter-rotation speed of 2º per minute (2θ). The identification of the phase composition of the samples was performed using the Match program (version 3)[35] and the X-ray database pdf-2 (ICDD). The solid solutions unit cell's parameters were computed using the FullProf Suite Package (3.0) program DICVOL. For the refinement crystal structure of solid solutions obtained by the Rietveld method, we used an experimental array of intensities and angles of reflection in the range of 15-140º (2θ) conducted by the electronically controlled diffractometer DRON-2. The exposure time at each point and the scanning steps were 3 seconds and 0.05º, respectively. Refinement was achieved using the FULLPROF.2k software (version 3.40)[36] with a graphical interface WinPLOTR included in the above software package. Calculating theoretical intensities and refinement of the unit cell's parameters, atomic coordinates, isotropic temperature parameters of atoms, and filling factors of correct point systems were performed using the FullProf.2k program (version May-2018) from the WinPLOTR software package.[37] The corresponding atoms' coordinates in the sodium lead apatite $Pb_8Na_2(PO_4)_6$ were used as initial data for the calculations.[38] Some samples were examined by scanning electron microscopy JSM-6490LV with an X-ray energy dispersive spectrometer (INCA Penta FETx3) to determine the grain size, elemental composition, and distribution of elements over the surface of the particles.

2.3. Procedure

The $Pb_{8-x}Sr_xNa_2(PO_4)_6$ solid solutions were synthesized by two methods: the first method was called **solid-state reaction** or **ceramic technology** when all samples were mixed while grinding in an agate mortar for 20–30 minutes. The mixtures were placed in alundum crucibles and calcined at 300 °C for 3 hours to remove volatile substances. The weight was 1 g. The synthesis conditions were provided by multistage calcination of the mixtures in the temperature range of 400–800 °C with intermediate grinding of the sinter every 100 °C. The essence of the second method called the precipitation method or semi-ceramic technology is the following: after weighing all samples of starting materials, each sample was placed in a 100 mL heat-resistant beaker and wetted with distilled water. Then 5 mL of concentrated nitric acid was added. The total volume of the resulting solution was brought up to 25–30 mL with distilled water. Complete dissolution of weighed portions of the starting materials was achieved with slight heating of the solution. After that, 2 mL of glycerol and approximately 1 g of ammonium nitrate were added to each resulting solution. The necessity of this stage lies in the fact that glycerin and ammonium nitrate contribute to an increase in friability and a decrease in adhesion to the walls of the charge glass, which is formed after the removal of the solvent. Water removal was carried out by slow evaporation during heating, in which the resulting solutions were maintained in a "pre-boiling" state. Each sample was calcined in a muffle furnace with a gradual increase in temperature to 500 °C to decompose intermediate products and remove gaseous substances. The solids were homogenized for 10 min in an agate mortar, placed in alundum crucibles, and then calcined at temperatures of 300 °C and 600 °C for 2 h to remove volatile substances. According to this method, the homogenization of the sample components was carried out in an aqueous solution with nitric acid. Compared with the

classical method, known as a solid-state reaction or ceramic technology, the advantage of "semi-ceramic technology" is the mixing of the component of the starting materials in a solution accomplished to a significantly greater extent than when grinding in a mortar or homogenization in a ball mill. Subsequently, the best degree of homogenization of the initial components leads to a decrease in the sample time of high-temperature calcination.

All samples synthesized by ceramic and semi-ceramic technologies were calcined at a temperature of 800 °C to reach a constant phase composition. After every 3-4 h of calcination at 800 °C, the samples were homogenized and analyzed by X-ray to monitor the reaction progress. The total calcined time at 800 °C was 23 h.

3. Results and Discussion

The X-ray phase analysis of $Pb_{(8-x)}Sr_xNa_2(PO_4)_6$ ($0 \le x \le 4$) solid solutions showed that the phase of the apatite structure is present in all synthesized samples' diffraction patterns (Fig. 1).

In the composition range $0 \le x \le 2.75$, diffractogram system $Pb_{8-x}Sr_xNa_2(PO_4)_6$ shows only reflections of the $NaPb_4(PO_4)_3$ phase (pure apatite). The compositions with x = 3.00 and 3.50, present reflections of the PbO and $NaSrPO_4$ phases besides the apatite reflections. The relative intensity of the reflections of these two phases increases with the increase in x. Fig. 2 shows the diffraction pattern of composition with x = 4.00 for the system $Pb_{8-x}Sr_xNa_2(PO_4)_6$ and X-ray diffraction patterns of the phases identified were created according to the pdf-2 database (ICDD). During the phase identification of apatite structure with x = 4.00, many reflections belong to other apatite phases besides pure apatite phases, such as $NaPb_4(PO_4)_3$, $Pb_5(PO_4)_3OH$, PbO, $NaPbPO_4$, and $NaSrPO_4$.

The formation of a single-phase for $Pb_{8-x}Sr_xNa_2(PO_4)_6$ system is confirmed by the composition with x = 2.00 and 2.50 using scanning electron microscopy. Fig. 3 shows a micrograph of a composition sample with x = 2.50.

The results obtained by scanning electron microscopy showed the formation of acceptable polycrystalline samples, for which the size of the aggregates is 3–10 microns and the size of individual grains is 1–3 microns. It should be noticed that chemical elements are spread uniformly throughout the particle surface (Figs. 4, 5). The expected theoretical composition of the obtained samples is in agreement with the calculated values (Table 1). We found no grains with different content of the main components.

Based on X-ray phase analysis and electron microscopy scanning, strontium substitution for lead in the $Pb_8Na_2(PO_4)_6$ compound, single-phase solid solutions are formed within the composition range with $0.00 \le x < 3.00$.

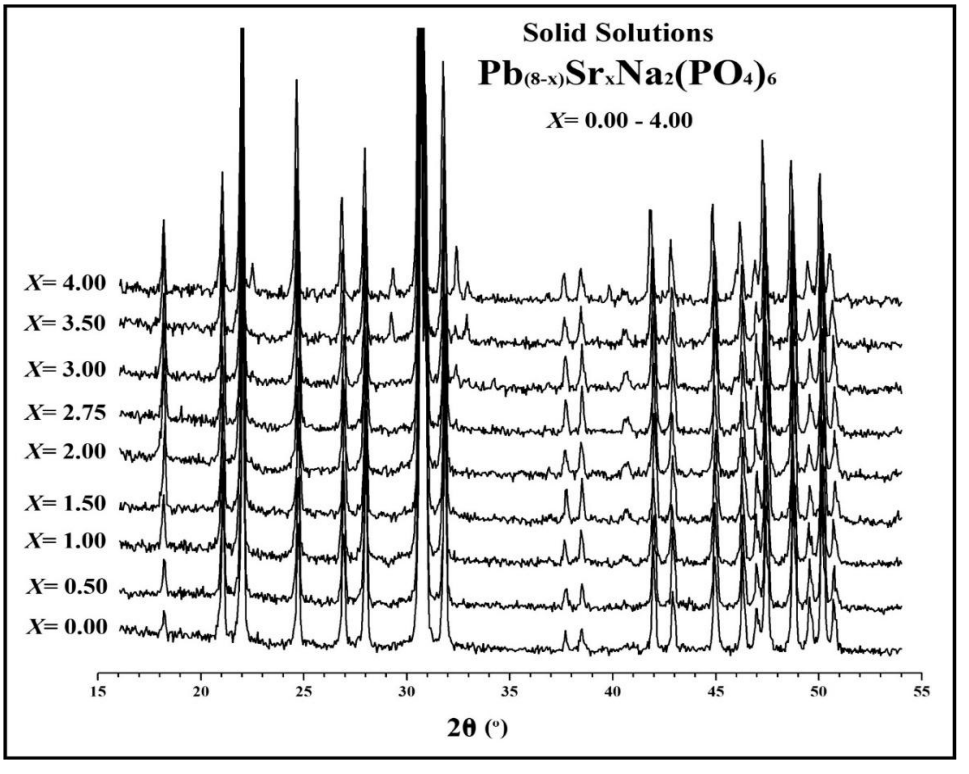

Fig. 1. X-ray System $Pb_{(8-x)}Sr_xNa_2(PO_4)_6$ diffraction patterns, all samples calcinated at 800 °C for 23 h

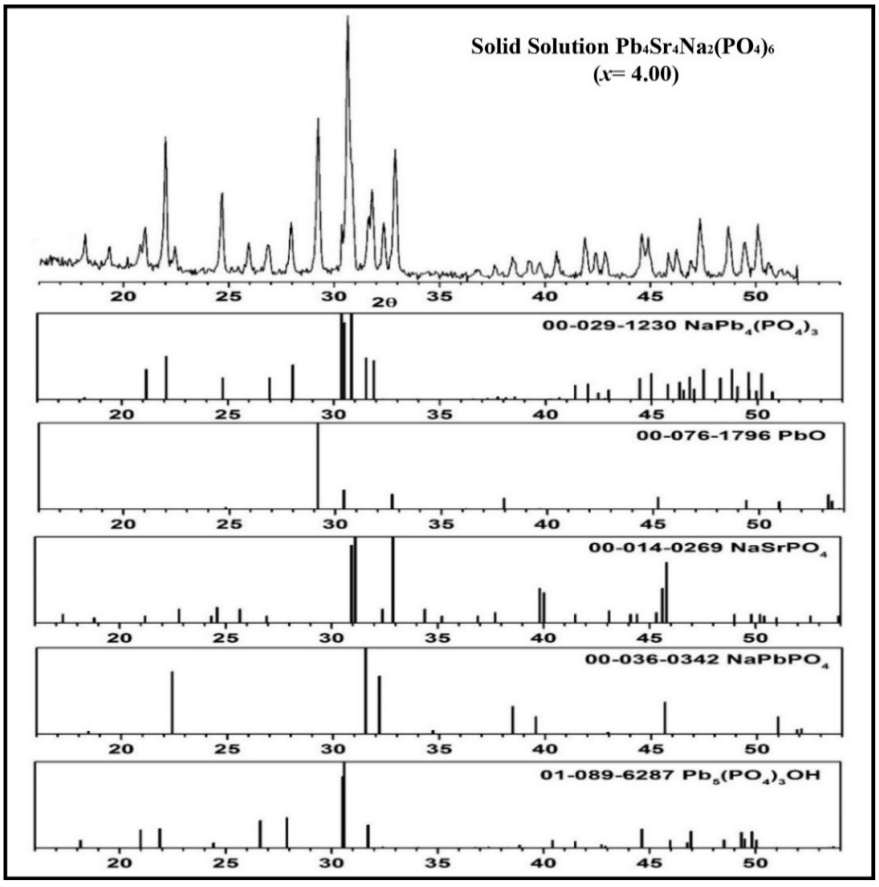

Fig. 2. The X-ray diffraction pattern $Pb_4Sr_4Na_2(PO_4)_6$ is based on the pdf-2 database (ICDD)

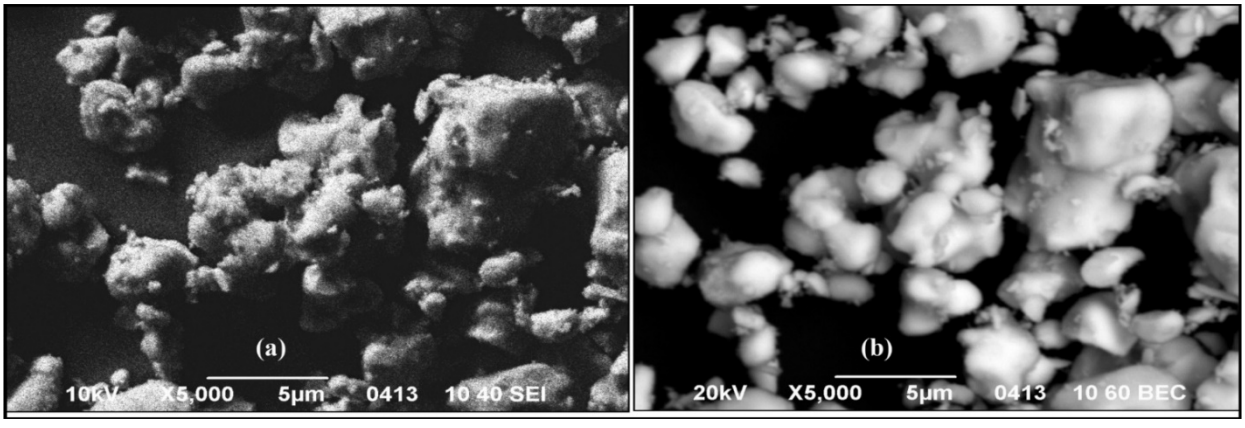

Fig. 3. (a) Micrograph of $Pb_6Sr_2Na_2(PO_4)_6$ composition, and (b) $Pb_{5.5}Sr_{2.5}Na_2(PO_4)_6$ composition (magnified 5000 times)

Table 1. SEM results of $Pb_{(8-x)}Sr_xNa_2(PO_4)_6$ with x=0.00, x=2.00 and x=2.50

Content, wt. %										
x	Pb		Na		Sr		P		O	
	Calcd[a]	found	Calcd[a]	found	Calcd[a]	found	Calcd[a]	found	Calcd[a]	found
0.00	22.3	20.0	5.7	5.0	-	-	14.8	15.0	57.2	60.0
2.00	15.2	15.0	7.2	5.0	5.1	5.0	14.2	15.0	58.3	60.0
2.50	14.1	13.8	6.9	5.0	6.2	6.2	13.7	15.0	59.1	60.0
[a] Calculated										

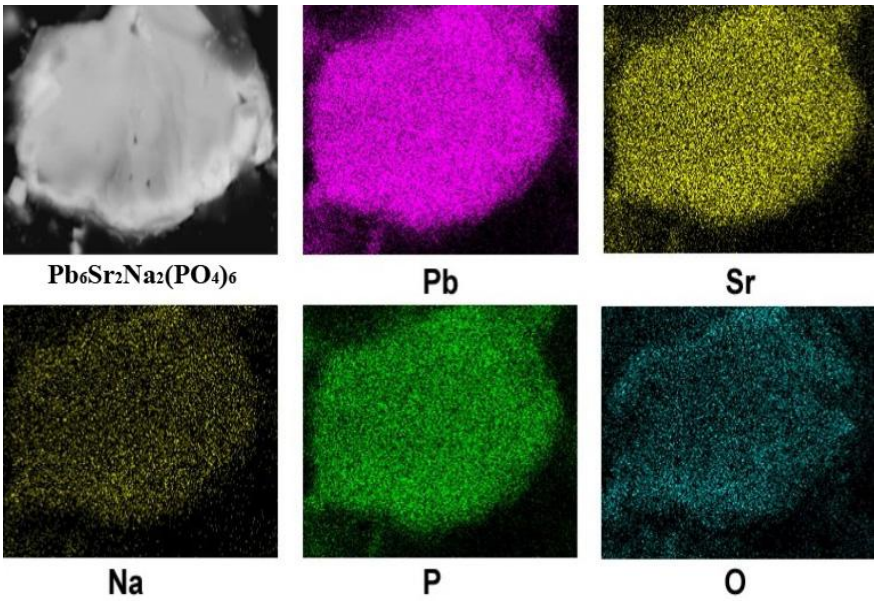

Fig. 4. Micrograph of $Pb_6Sr_2Na_2(PO_4)_6$ composition and the distribution of elements on its surface, obtained by X-ray phase analysis

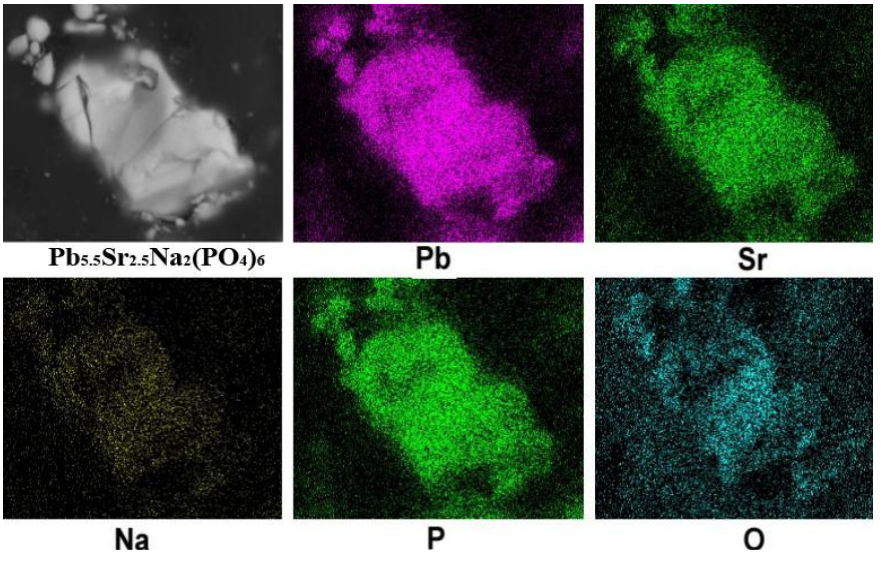

Fig. 5. Micrograph of $Pb_{5.5}Sr_{2.5}Na_2(PO4)_6$ composition and diffusion of elements on its surface, obtained by X-ray phase analysis

The isomorphic isovalent substitution of lead for strontium is accompanied by a change in the parameters of the elementary hexagonal cell of the apatite structure dependent on the strontium content in the solid solution structure. This dependence is shown in Fig. 6. The change in the cell parameter *a* is within the same determined range, whereas in the single-phase area the value of the cell parameter *c* decreases linearly with increasing strontium content in the solid solution.

Refinement of the crystal structure properties for solid solutions $Pb_{(8-x)}Sr_xNa_2(PO_4)_6$ was conducted for the sample compositions with x = 0.00, 1.00, 2.00, and 2.75. Two cationic positions M1 and M2 of the apatite structure are "claimed" by three different cations (Na^+, Sr^{2+}, and Pb^{2+}) in the crystal structure of strontium-containing solid solutions. Therefore, their positional distribution cannot be determined without introducing other locations/assumptions. Based on this, when calculating the occupancy of cationic positions in the structure of $Pb_{(8-x)}Sr_xNa_2(PO_4)_6$ solid solutions, the following provisions were first taken into account: 1) all the elements included in the sample are in ionic form; 2) the principle of elec-

troneutrality is observed; 3) cation positions M (1) and M (2) must be filled and not contain vacancies. Assessment of the "correctness" of calculating the distribution of cations was carried out by the reliability factors and the "adequacy" of the values of the isotropic thermal parameters of the atoms. Second, one cation occupancy at position M (1) or M (2) was recorded since the distribution of only two cations between two positions could be calculated. M–O bonds in the M (1) polyhedron are predominantly ionic ones in the crystal structure of the $Pb_8Na_2(PO_4)_6$ compound, and in the M (2) polyhedron they are covalent. In addition to the ionic nature of the Na – O, Sr – O bonds and the covalent nature of the Pb – O bond, the most likely situation is when Na^+ and Sr^{2+} ions are localized in the M1 cationic position and Pb^{2+} ions are localized in the M2 cationic position.[39, 40]

When refining $Pb_{(8-x)}Sr_xNa_2(PO_4)_6$ crystal structure, different variants to fixate the occupations of cations M (1) and M (2) positions were used, and "adequate" results were obtained in the following cases:

Assumption 1: in the structure of solid solution $Pb_{(8-x)}Sr_xNa_2(PO_4)_6$ sodium atoms are distributed in the same way as in the $Pb_8Na_2(PO_4)_6$ structure, and the occurrence of strontium ions does not affect the redistribution of sodium ions;

Assumption 2: Sr^{2+} ions are localized only in position M (1) of apatite structure, and the Na^+ and Pb^{2+} ions are distributed between two cation sites.

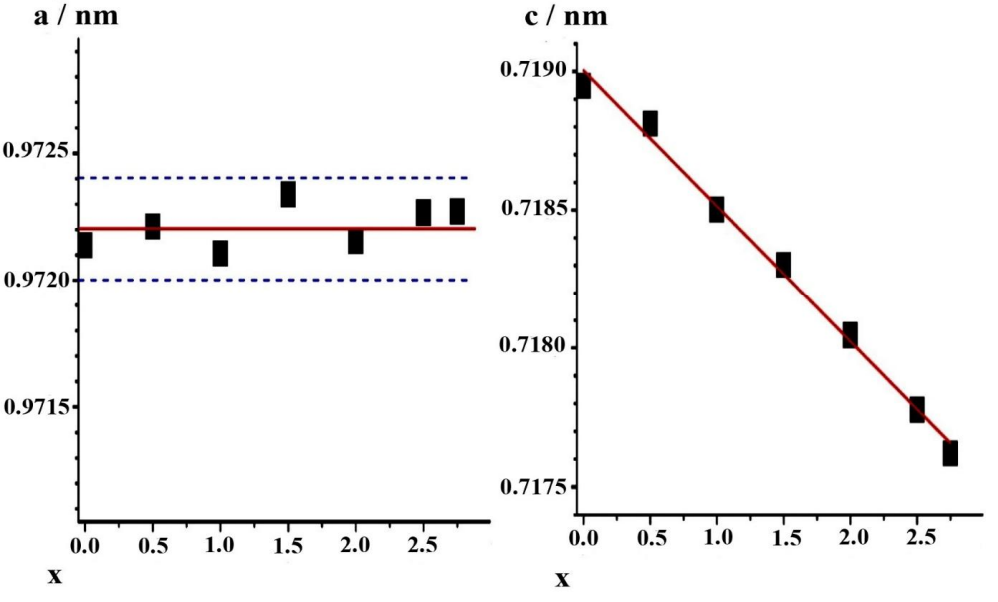

Fig. 6. The *a* and *c* unit cell parameters *versus* the substitution limit in the $Pb_{(8-x)}Sr_xNa_2(PO_4)_6$

Table 2. Site occupancy of cationic positions and reliability factors in the structure $Pb_{5.25}Sr_{2.75}Na_2(PO_4)_6$

	Assumption 1	Assumption 2
Pb(1) (4f)	0.81(2)	0.64(2)
Na(1) (4f)	1.86	0.61(2)
Sr(1) (4f)	1.43(2)	2.75
Pb(2) (6h)	4.45(2)	4.61(2)
Na(2) (6h)	0,14	1.39(2)
Sr(2) (6h)	1.41(2)	0.00
RB	7.70	7.70
RF	7.63	6.78
RP	6.41	6.41
RWP	8.20	8.19
$\chi 2$	1.39	1.38

Table 3. Isotropic thermal parameters of atoms in the system $Pb_{5.25}Sr_{2.75}Na_2(PO_4)_6$

Atom	Assumption 1	Assumption 2
M (1)	1.2(2)	1.1(2)
M (2)	0.77(6)	0.78(6)
P	2.7(4)	2.7(4)
O	3.1(5)	3.1(5)

Table 4. Selected Mean Interatomic Distances (Å) in the system $Pb_{5.25}Sr_{2.75}Na_2(PO_4)_6$

Interatomic Distances, Å	Assumption 1	Assumption 2
M(1)–O(1) × 3	2.47(3)	2.46(3)
M(1)–O(2) × 3	2.61(4)	2.61(4)
M(1)–O(3) × 3	2.80(3)	2.80(3)
<Pb(1)–O(1-3)>	2.63	2.62
M(2)–O(1)	2.78(3)	2.78(3)
M(2)–O(2)	2.17(4)	2.17(4)
M(2)–O(3) × 2	2.46(2)	2.46(2)
M(2)–O(3) × 2	2.57(3)	2.57(4)
<M(2)–O(1-3)>	2.50	2.50
P–O(1)	1.51(5)	1.53(5)
P–O(2)	1.53(4)	1.53(4)
P–O(3) × 2	1.61(3)	1.60(3)
<P–O>	1.56	1.56

Table 5. Site occupancy of cationic positions and reliability factors in the solid solution $Pb_{(8-x)}Sr_xNa_2(PO_4)_6$

	x = 0.00	x = 1.00	x = 2.00	x = 2.75
Pb(1) (4f)	2.14(2)	1.14(2)	0.41(3)	0.64(2)
Na(1) (4f)	1.86(2)	1.86(2)	1.59(3)	0.61(2)
Sr(1) (4f)	-	1.0	2.0	2.75
Pb(2) (6h)	5.86(2)	5.86(2)	5.59(3)	4.61(2)
Na(2) (6h)	0.14(2)	0.14(2)	0.41(3)	1.39(2)
Sr(2) (6h)	-	0	0	0
RB	6.16	6.37	9.51	7.70
RF	6.34	5.87	8.42	6.78
RP	6.55	6.43	7.06	6.41
RWP	8.32	8.23	8.92	8.19
χ^2	1.44	1.30	1.63	1.38

Table 6. Selected Mean Interatomic Distances (Å) in the system $Pb_{(8-x)}Sr_xNa_2(PO_4)_6$

Interatomic Distances, Å	x = 0.00	x = 1.00	x = 2.00	x = 2.75
M(1)–O(1) × 3	2.43(2)	2.45(4)	2.45(4)	2.46(3)
M(1)–O(2) × 3	2.75(3)	2.68(4)	2.65(4)	2.61(4)
M(1)–O(3) × 3	2.80(2)	2.85(2)	2.82(3)	2.80(3)
<M(1)–O(1-3)>	2.66	2.66	2.64	2.62
M(2)–O(1)	2.82(3)	2.79(4)	2.80(4)	2.78(3)
M(2)–O(2)	2.21(3)	2.17(4)	2.16(4)	2.17(4)
M(2)–O(3) × 2	2.50(2)	2.50(2)	2.46(3)	2.46(2)
M(2)–O(3) × 2	2.52(2)	2.56(3)	2.55(4)	2.57(4)
<M(2)–O(1-3)>	2.51	2.51	2.50	2.50
P–O(1)	1.45(4)	1.52(5)	1.51(6)	1.53(5)
P–O(2)	1.52(3)	1.55(4)	1.55(5)	1.53(4)
P–O(3) × 2	1.63(2)	1.61 (4)	1.59(5)	1.60(3)
<P–O>	1.56	1.57	1.56	1.56

It should be noted that the given assumptions (the position M (1) is occupied only with Na^+ and Sr^{2+} ions and Na^+ ions or Sr^{2+} ions are localized exclusively in the M (2) position in the compositions with x = 2.00 and 2.75) did not give a positive result in calculations. The calculations revealed that the crystal structure characteristics of solid solutions refined using Assumption 1 and Assumption 2 led to almost identical results regarding the values of reliability factors, isotropic thermal parameters, and interatomic distances. Tables 2, 3, and 4 compare X-ray data results of the structure $Pb_{5.25}Sr_{2.75}Na_2(PO_4)_6$.

Based on the X-ray structural analysis results, it is assumed that lead (Pb) is predominantly located in the M (2) region, while sodium (Na) and strontium (Sr) atoms are statistically distributed between the M (1) and M (2) cationic region.

Occupation of crystallographic positions, as well as values of interatomic distances for samples of the system $Pb_{(8-x)}Sr_xNa_2(PO_4)_6$ (based on the results of assumption 2), are presented in Tables 5 and 6. Analysis of the change in interatomic distances shows that the entrance of strontium ions into the structure of the solid solution leads to a decrease in the distance M (1) – O (2), which affects the tendency to decrease average M – O distances in the M (1) polyhedron coordination. The mean interatomic distances in the M (2) coordination polyhedrons and the PO_4 tetrahedra remain unchanged with the changes in the solid solution composition.

4. Conclusions

In this work, $Pb_{(8-x)}Sr_xNa_2(PO_4)_6$ solid solutions were synthesized at 800 °C for 23 h and examined by several techniques: X-Ray Diffraction (XRD), Electron Microscopy Scanning (SEM), and Rietveld refinement techniques. Specifically, the effects of substitution within the crystal structure of solid solutions were studied. This allowed to predict the behavior of luminescent properties in various apatites. In the $Pb_8Na_2(PO_4)_6$ structure, the strontium substitution boundaries for lead occurred in the composition range of 0.00 to 2.75 (pure apatite), whereas the compositions $Pb_5Sr_3Na_2(PO_4)_6$, $Pb_{4.5}Sr_{3.5}Na_2(PO_4)_6$, and $Pb_4Sr_4Na_2(PO_4)_6$ show many reflections belonging to other apatite phases such as $NaPb_4(PO_4)_3$, $Pb_5(PO_4)_3OH$, PbO, $NaPbPO_4$, and $NaSrPO_4$. The electron microscopy scanning and the predicted theoretical composition of solid solution samples for compositions $Pb_8Na_2(PO_4)_6$, $Pb_6Sr_2Na_2(PO_4)_6$, and $Pb_{5.5}Sr_{2.5}Na_2(PO_4)_6$, were evaluated satisfactorily.

The lattice unit cell parameters show that the change in cell parameter *a* is within the accuracy of the calculated values, while the values of cell parameter *c* decreases slightly with increasing strontium content in the solid solution. The reason is that strontium (Sr) has no $6S^2$ orbital (electron pair), while lead (Pb) has. The lone pair has a negative charge, and oxygen anions are located around cations. Therefore, there is repulsion between a lone pair and anions.

For $Pb_{(8-x)}Sr_xNa_2(PO_4)_6$ solid solutions the refinement of the crystal structure characteristics was carried out for sample compositions with x = 0.00, 1.00, 2.00, and 2.75. It was concluded that lead (Pb) is mainly localized in the M (2) position while the sodium (Na) and strontium (Sr) atoms are allocated between the M (1) and M (2) cationic positions. Also, as substitution increases, a change in the occupancy of positions occurs by most sodium ions, which move from position M (1) to position M (2). The obtained results can be important for developing new technical materials with a lead sodium apatite structure.

Conflict of Interests

The researchers announced that publishing this paper does not entail a conflict of interest.

Acknowledgments

We thank all the assistance in preparing, analyzing, and examining the samples in this paper.

References

[1] Ptáček P.; Apatites and their Synthetic Analogues – Synthesis, Structure, Properties and Applications; IntechOpen, 2016. https://doi.org/10.5772/62212

[2] Fiume, E.; Magnaterra, G.; Rahdar, A.; Verné, E.; Baino, F. Hydroxyapatite for Biomedical Applications: A Short Overview. *Ceramics* **2021**, *4*, 542–563. https://doi.org/10.3390/ceramics4040039

[3] Al-Eesaa, N.A.; Johal, A.; Hill, R.G.; Wong, F.S.L. Fluoride Containing Bioactive Glass Composite for Orthodontic Adhesives – Apatite Formation Properties. *Dent. Mater.* **2018**, *34*, 1127–1133. https://doi.org/10.1016/j.dental.2018.04.009

[4] Nur, A.; Budiman, A.W.; Jumari, A.; Nazriati, N.; Fajaroh, F. Electrosynthesis of Ni-Co/Hydroxyapatite as a Catalyst for Hydrogen Generation *via* the Hydrolysis of Aqueous Sodium Borohydride ($NaBH_4$) Solutions. *Chem. Chem. Technol.* **2021**, *15*, 389–394. https://doi.org/10.23939/chcht15.03.389

[5] Abdul Jabar, M.A.B.; Ignatov, A.V. New Synthesis of Solid-Solution Lead Hydroxyapatite (PbHAP) by Ceramic and Semi-Ceramic Methods. *J. Chem. Soc. Pak.* **2020**, *42*, 363–268. https://jcsp.org.pk/issueDetail.aspx?aid=9c56ea37-f765-416d-b62f-9ba5f29c8b3f

[6] Abdel-Aal, E.A.; Abdel-Ghafar, H.M.; El-Sayed, D.; Ewais, E.M. Synthesis of High Hardness Hydroxyapatite Particles Using

Surfactant Assisted Hydrothermal Method. *Int. J. Innov. Sci. Technol.* **2022**, *2*, 35–50. https://doi.org/10.21608/IJMTI.2022.115060.1044
[7] Parajuli, K.; Malla, K.P.; Panchen, N.; Ganga, G.C.; Adhikari, R. Isolation of Antibacterial Nano-Hydroxyapatite Biomaterial from Waste Buffalo Bone and Its Characterization. *Chem. Chem. Technol.* **2022**, *16*, 133–141. https://doi.org/10.23939/chcht16.01.133
[8] Abdul Halim, N.A.; Hussein, M.Z.; Kandar, M.K. Nanomaterials-Upconverted Hydroxyapatite for Bone Tissue Engineering and a Platform for Drug Delivery. *Int. J. Nanomedicine* **2021**, *16*, 6477–6496. https://doi.org/10.2147/IJN.S298936
[9] Combes, C.; Cazalbou, S.; Rey, C. Apatite Biominerals. *Minerals* **2016**, *6*, 34. https://doi.org/10.3390/min6020034
[10 Deng, S.; Lin, Z.; Tang, H.; Ullah, S.; Bi, Y. Rapid Synthesis of Hydroxyapatite Nanoparticles *via* a Novel Approach in the Dual-Frequency Ultrasonic System for Specific Biomedical Application. *J. Mater. Res.* **2019**, *34*, 2796–2806. https://doi.org/10.1557/jmr.2019.119
[11] Iconaru, S.L.; Motelica-Heino, M.; Guegan, R.; Beuran, M.; Costescu, A.; Predoi, D. Adsorption of Pb (II) Ions onto Hydroxyapatite Nanopowders in Aqueous Solutions. *J. Mater.* **2018**, *11*, 2204–2221. https://doi.org/10.3390/ma11112204
[12] Xin, Y.; Shirai, T. Noble-Metal-Free Hydroxyapatite Activated by Facile Mechanochemical Treatment Towards Highly-Efficient Catalytic Oxidation of Volatile Organic Compound. *Sci Rep* **2021**, *11*, 7512. https://doi.org/10.1038/s41598-021-86992-8
[13] Ebadipour, N.; Paul, S.; Katryniok, B.; Dumeignil, F. Calcium Hydroxyapatite: A Highly Stable and Selective Solid Catalyst for Glycerol Polymerization. *Catalysts* **2021**, *11*, 1247. https://doi.org/10.3390/catal11101247
[14] Antao, S.M.; Dhaliwal, I. Lead Apatites: Structural Variations among $Pb_5(BO_4)_3Cl$ with B = P (Pyromorphite), As (Mimetite) and V (Vanadinite). *J Synchrotron Radiat* **2018**, *25*, 214–221. https://doi.org/10.1107/S1600577517014217
[15] Khademolhosseini, M.R.; Mobasherpour, I.; Ghahreman, D. Lead Adsorption by Nano-Hydroxyapatite Granules in a Fixed-Bed Column. *Chem. Chem. Technol.* **2018**, *12*, 372–378. https://doi.org/10.23939/chcht12.03.372
[16] Bratychak Jr, M.; Chopyk, N.; Zemke, V. Effect of Hydroxyapatite on the Glue Line Strength of the Compositions Containing Polyvinylpirrolidone. *Chem. Chem. Technol.* **2016**, *10*, 473–478. https://doi.org/10.23939/chcht10.04.473
[17] Zhu, Y.; Huang, B.; Zhu, Z.; Liu, H.; Huang, Y.; Zhao, X.; Liang, M. Characterization, Dissolution and Solubility of the Hydroxypyromorphite–Hydroxyapatite Solid Solution $[(Pb_xCa_{1-x})_5(PO_4)_3OH]$ at 25 °C and pH 2-9. *Geochemical Trans.* **2016**, *17*, 2. https://doi.org/10.1186/s12932-016-0034-8
[18] Giera, A.; Manecki, M.; Bajda, T.; Rakovan, J.; Kwaśniak-Kominek, M.; Marchlewski, T. Arsenate Substitution in Lead Hydroxyl Apatites: A Raman Spectroscopic Study. *Spectrochim. Acta A Mol. Biomol. Spectrosc.* **2016**, *152*, 370–377. https://doi.org/10.1016/j.saa.2015.07.015
[19] Hopwood, J.D.; Derrick, G.R.; Brown. D.R.; Newman, C.D.; Haley, J.; Kershaw, R.; Collinge, M. The Identification and Synthesis of Lead Apatite Minerals Formed in Lead Water Pipes. *J. Chem.* **2016**, *2016*, 9074062. https://doi.org/10.1155/2016/9074062
[20] Bulanov, E.N.; Petrov, S.S.; Knyazev, A.V. New Iodine-Apatites: Synthesis and Crystal Structure. *Turk. J. Chem.* **2021**, *45*, 1444–1453. https://doi.org/10.3906/kim-2102-5
[21] Mohd Pu'ad, N.A.S.; Koshy, P.; Abdullah, H.Z.; Idris, M.I.; Lee, T.C. Syntheses of Hydroxyapatite from Natural Sources. *Heliyon* **2019**, *5*, 01588. https://doi.org/10.1016/j.heliyon.2019.e01588
[22] Garibay-Alvarado, J.A.; Herrera-Ríos, E.B.; Vargas-Requena, C.L.; Ruíz-Baltazar, Á.J.; Reyes-López, S.Y. Cell Behavior on Silica-Hydroxyapatite Coaxial Composite. *PLoS One* **2021**, *16*, 0246256. https://doi.org/10.1371/journal.pone.0246256
[23] Pokhrel, S. Hydroxyapatite: Preparation, Properties and its Biomedical Applications. *Adv. Chem. Engineer. Sci.* **2018**, *8*, 225–240. https://doi.org/10.4236/aces.2018.84016
[24] Sari, M.; Hening, P.; Chotimah; Ana, I.D.; Yusuf, Y. Bioceramic Hydroxyapatite-Based Scaffold with a Porous Structure Using Honeycomb as a Natural Polymeric Porogen for Bone Tissue Engineering. *Biomater. Res.* **2021**, *25*, 2. https://doi.org/10.1186/s40824-021-00203-z
[25] Skwarek, E.; Janusz, W.; Sternik, D. The Influence of the Hydroxyapatite Synthesis Method on the Electrochemical, Surface and Adsorption Properties of Hydroxyapatite. *Adsorp. Sci. Technol.* **2017**, *35*, 507–518. https://doi.org/10.1177/0263617417698966
[26] Ruphuy, G.; Weide, T.; Lopes, J.C.B.; Dias, M.M.; Barreiro, M.F. Preparation of Nano-Hydroxyapatite/Chitosan Aqueous Dispersions: From Lab Scale to Continuous Production Using an Innovative Static Mixer. *Carbohydr. Polym.* **2018**, *202*, 20–28. https://doi.org/10.1016/j.carbpol.2018.08.123
[27] Afifi, M.; El-Naggar, M.E.; Muhammad, S.; Alghamdi, N.A.; Wageh, S.; Salem, S.R.; Alhashmialameer, D.; Taleb, M.A. Nanocomposites Based on Hydroxyapatite/Lithium Oxide and Graphene Oxide Nanosheets for Medical Applications. *J. Mater. Sci.* **2022**, *57*, 11300–11316. https://doi.org/10.1007/s10853-022-07342-1
[28] Sboui, N.; Agougui, H.; Jabli, M.; Boughzala, K. Synthesis, Physico-Chemical, and Structural Properties of Silicate Apatites: Effect of Synthetic Methods on Apatite Structure and Dye Removal. *Inorg. Chem. Commun.* **2022**, *142*, 109628. https://doi.org/10.1016/j.inoche.2022.109628
[29] Get'man, E.I.; Loboda, S.N.; Ignatov, A.V.; Prisedsky, V.V.; Abdul Jabar, M.A.B.; Ardanova, L.I. Isomorphous Substitution of Rare-Earth Elements in Lacunary Apatite $Pb_8Na_2(PO_4)_6$. *J. Am. Chem. Soc.* **2016**, *55*, 2165–2173. https://doi.org/10.1021/acs.inorgchem.5b02571
[30] Abdul Jabar, M.A.B.; Get'man, E.I.; Ignatov, A.V. New Gadolinium-Substituted Lead Sodium Apatite Structure. *Funct. Mater.* **2018**, *25*, 713–719. https://doi.org/10.15407/fm25.04.713
[31] Rafie, S.M.M.; Nordin, D. Synthesis and Characterization of Hydroxyapatite Nanoparticle. *Malays. J. Anal. Sci.* **2017**, *21*, 136–148. http://dx.doi.org/10.17576/mjas-2017-2101-16
[32] Li, Y.; Chen. C.; Jin, M.; Xiang, J.; Tang, J.; Zhao, X.; Zheng, J.; Guo, C. Multi-Mode Excited $Cs_2NaBiCl_6$ Based Double Perovskite Phosphor for Anti-Counterfeiting. *J. Lumin.* **2022**, *247*, 118915. https://doi.org/10.1016/j.jlumin.2022.118915
[33] Abudoureheman, M.; Han, S.; Dong, X.; Lei, B.; Wang, Y.; Yang, Z.; Long, X.; Pan, S. Syntheses, Characterization and Theoretical Studies of Three Apatite-Type Phosphates $MPb_4(PO_4)_3$ (M = K, Rb, Cs). *J. Alloys Compd.* **2017**, *690*, 330–336. https://doi.org/10.1016/j.jallcom.2016.08.115
[34] Mohammad, A.M.; Salah Eldin, T.A.; Hassan, A.M.; El-Anadouli, B.E. Efficient Treatment of Lead-Containing Wastewater by Hydroxyapatite/Chitosan Nanostructures. *Arab. J. Chem.* **2017**, *10*, 683–690. https://doi.org/10.1016/j.arabjc.2014.12.016
[35] Chen, D.; Zhao, J.; Jiang, X. Synthesis and Characterization of Silver Substituted Strontium Phosphate Silicate Apatite Using Solid-

State Reaction for Osteoregenerative Applications. *J. Bioeng.* **2021**, *12*, 1111–1125. https://doi.org/10.1080/21655979.2021.1899670
[36] El Hayek, E.; El Samrani, A. Lartiges, B.; Kazpard, V.; Aigouy, T. Lead Bioaccumulation in *Opuntia ficus-indica* Following Foliar or Root Exposure to Lead-Bearing Apatite. *Environ. Pollut.* **2017**, *220*, 779–787. https://doi.org/10.1016/j.envpol.2016.10.046
[37] Coulon, A.; Laurencin, D.; Grandjean, A.; Gallet, S.L.; Minier, L.; Rossignol, S.; Campayo, L. Key Parameters for Spark Plasma Sintering of Wet-Precipitated Iodate-Substituted Hydroxyapatite. *J. Eur. Ceram. Soc.* **2016**, *36*, 2009–2016. https://doi.org/10.1016/j.jeurceramsoc.2016.02.041
[38] Tite, T.; Popa, A.; Balescu, L.M.; Bogdan, I.M.; Pasuk, I.; Ferreira, J.M.F.; Stan, G.E. Cationic Substitutions in Hydroxyapatite: Current Status of the Derived Biofunctional Effects and they're *in vitro* Interrogation Methods. *J. Mater.* **2018**, *11*, 2081. https://doi.org/10.3390/ma11112081
[39] Bulanov, E.N.; Knyazev, A.V.; Lelet, M.I. Thermodynamic Modeling of Integration of Strontium into Bone Tissue Hydroxyapatite. *J. Solid State Chem.* **2017**, *1*, 42–47. https://doi.org/10.18572/2619-0141-2017-1-1-42-47
[40] Venkatesan, S.; Hassan, M.; Ryu, H.J. Adsorption and Immobilization of Radioactive Ionic-Corrosion-Products Using Magnetic Hydroxyapatite and Cold-Sintering for Nuclear Waste Management Applications. *J. Nucl. Mater.* **2019**, *514*, 40–49. https://doi.org/10.1016/j.jnucmat.2018.11.026

Received: May 28, 2023 / Revised: July 09, 2022 / Accepted: December 15, 2022

НОВІ ТВЕРДІ РОЗЧИНИ ЗАМІЩЕННЯ СТРОНЦІЮ (Sr) ПЛЮМБУМОМ (Pb) У СТРУКТУРІ АПАТИТІВ

Анотація. *Заміщення стронцію на плюмбум у $Pb_{(8-x)}Sr_xNa_2(PO_4)_6$ проаналізовано з використанням XRD, SEM та методу Рітвельда. Усі зразки були синтезовані з використанням керамічних і напівкерамічних технологій. Чистий апатит утворювався в складі від x=0,00 до x=2,75. Результати свідчать про те, що зібрані склади зразків узгоджуються з розрахованими величинами.*

Ключові слова: *плюмбум, апатит, кераміка, напівкераміка, твердий розчин.*